THE JOURNAL OF PHYSICAL CHEMISTRY B

ARTICLE

pubs.acs.org/JPCB

Dissipative Structure Formation in Lipid/Lipopolymer Monolayers

Peter C. Seitz,[†,‡] Michael Reif,[§] Kenichi Yoshikawa,[‡] Rainer Jordan,[§,⊥] and Motomu Tanaka*[,†]

[†]Physical Chemistry of Biosystems, Institute of Physical Chemistry, University of Heidelberg, 69120 Heidelberg, Germany

[‡]Department of Physics, Graduate School of Science, Kyoto University, Kyoto, Japan

[§]Wacker-Lehrstuhl für Makromolekulare Chemie, Department Chemie, Technische Universität München, 85748 Garching, Germany

[⊥]Department Chemie, Technische Universität Dresden, 01069 Dresden, Germany

Supporting Information

ABSTRACT: We study the formation of dissipative microstructures in monomolecular films of surfactant mixtures, which occur near the three-phase contact line during Langmuir−Blodgett transfer onto a solid substrate. Continuous stripes parallel to the transfer direction are generated over several centimeters, indicating the phase separation of phospholipids and lipids with polymer head groups (lipopolymers). The systematic variation of transfer conditions revealed that transfer speed and subphase viscosity determine the stripe-to-stripe distance from several micrometers to submicrometers. To account for the physical mechanism of such pattern formation, we characterize the local film thickness and the membrane composition in the vicinity of the three-phase contact line using imaging ellipsometry and fluorescence microscopy. At relatively slow rates of substrate lifting, the power law exponent that we found between the interstripe distance and the transfer speed suggests that the stripe formation is due to spinodal decomposition, which can be accounted under the framework of the Cahn−Hilliard equation, whereas at relatively high rates, the distance is found to be proportional to the substrate speed, suggesting a dominant effect of the shear force on the stripe formation.

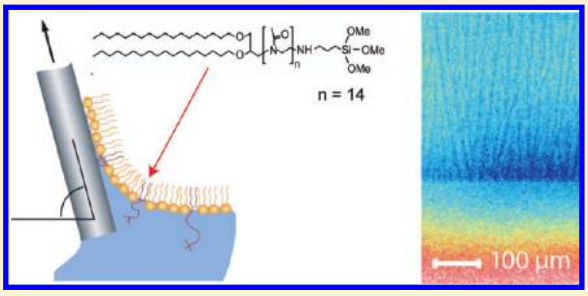

INTRODUCTION

The cell membrane is a fundamental building block of biological cells that serves as a boundary to separate intra- and extra-cellular spaces. The use of artificial model membranes enables one to quantitatively model the structures and functions of biological membranes with a small number of components. After the simplest and conventional "fluid mosaic model" proposed by Singer and Nicholson,[1] many experimental studies evidenced that lipids and proteins are not always uniformly mixed in membranes but can form static or dynamic domains, ranging over various length scales.[2,3] Heterogeneity has been observed in experiments, but technical limitations in the observations make it likely that much more is yet to be discovered.[4] From a physical viewpoint, biological membranes can be generalized as complex fluid membranes whose deformation is both plastic and elastic. However, in contrast to numerous studies that have reported dissipative pattern formation in polymer films out of equilibrium,[5,6] the formation of dynamic patterns in biological membrane models has hardly been studied so far.

To investigate the formation of static and dynamic structures in biological membranes, the deposition of planar lipid membranes on solid substrates (called solid-supported membranes) can offer unique advantages owing to their capability of coating macroscopically large areas.[7,8] The highly controllable preparation process using a Langmuir−Blodgett (LB) transfer enables the production of asymmetric membranes analogous to the originals found in nature. A first issue, the proximity of the membrane to the solid support can be resolved either by bedding of the membrane on a preformed polymer cushion or by separating the membrane from the solid substrate via linear polymer spacers (polymer-tethered membranes).

Along with the latter strategy, we reported that biological membrane models incorporating lipids functionalized with hydrophilic, linear poly(2-oxazoline) head groups (lipopolymers) can provide a thicker water reservoir to avoid direct membrane−substrate contacts.[9−13] In fact, the systematic variation of polymer chain length and molar fraction of lipopolymers allows for the fine adjustment of the interplay of interfacial forces[14] as well as the homogeneity and frictional environments of transmembrane integrin receptors.[15]

In our previous study, we found that the mixture of lipopolymers and matrix lipids could form a regular stripe pattern after the transfer from the air/water interface. Selective fluorescence labeling of lipids and lipopolymers confirmed that the stripe pattern perpendicular to the meniscus coincides with the demixing of lipids and lipopolymers.[16] The emerging structure is capable of incorporating transmembrane proteins (human platelet integrin $\alpha_{IIb}\beta_3$ receptors) into the lipopolymer-rich phase, which can serve as selective adhesion sites for target cells. Moreover, our experimental results demonstrated

Received: November 8, 2010
Revised: January 5, 2011
Published: February 22, 2011

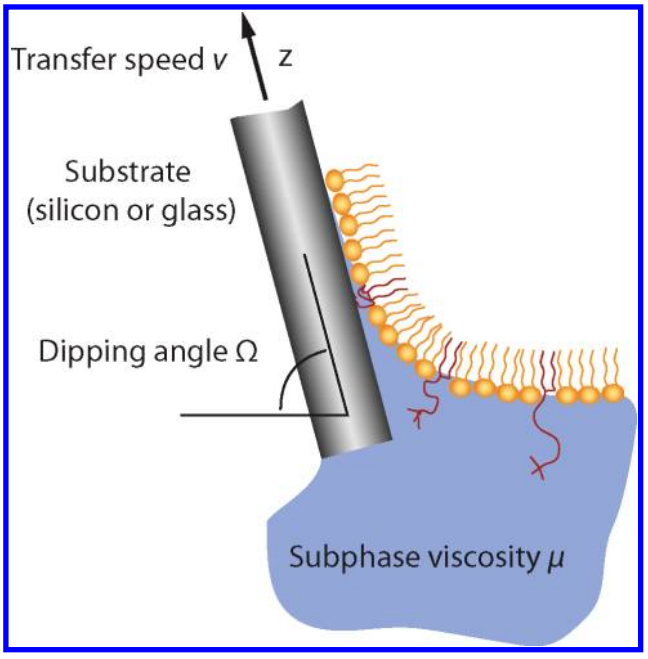

Figure 1. Schematic view of the transfer of a lipid/lipopolymer monolayer from the air/water interface. Three key parameters (the transfer speed, v; the subphase viscosity, μ; and the dipping angle, Ω) were varied to modulate the stripe pattern. It was confirmed that lipids and lipopolymers are homogeneously mixed before the transfer. Inset: Chemical structure of the lipopolymer DS-PMOx14-Si.

a clear influence of viscous friction near the three phase contact line on the stripe periodicity, suggesting that more quantitative measurements of the height profile in the vicinity of the wetting front are prerequisite.

In this study, we coupled a Langmuir film balance to a fluorescence microscope and an imaging ellipsometer to resolve the height profiles of the monolayer during the transfer with a vertical resolution of approximately nanometers and the lateral resolution of approximately micrometers. To regulate the dissipation of the film near the contact line, three parameters were varied systematically: the transfer speed, the subphase viscosity, and the dipping angle (see Figure 1). Throughout this study, the average distance between neighboring stripes (periodicity) is used to test the theoretical modeling.

MATERIALS AND METHODS

Materials. Glass cover slides (Menzel, Braunschweig, Germany) with a size of 25 mm × 75 mm and silicon wafers (Si-Mat, Landsberg am Lech, Germany) with native oxide (≈15 Å) were used as substrates. Both substrates were cleaned using a modified RCA protocol:[17] The samples were sonicated for 5 min in acetone, ethanol, methanol and purified water, followed by half an hour in a (1:1:5) mixture by volume of (30% ammonia/30% hydrogen peroxide/purified water) at 60 °C. After intensive rinsing with deionized water (GenPure, TKA, Niederelbert, Germany), the samples were dried in vacuum. 1-Stearoyl-2-oleoyl-*sn*-glycero-3-phosphatidylcholine (SOPC) was purchased from Avanti Polar Lipids (Alabaster, AL). The synthesis of poly (2-methyl-2-oxazoline) lipopolymer (DS-PMOx14-Si, Figure 1) is reported elsewhere.[9,18,19] Also in this case, the end-group functionalization of the polymer with trimethoxysilane groups for surface attachment and stable ether lipids was quantitative as confirmed by ^{1}H NMR spectroscopy. MALDI-TOF mass spectrometry and gel permeation chromatography measurements showed a narrow and monomodal mass distribution. End group analysis based on ^{1}H NMR spectroscopy data and MALDI-TOF mass spectrometry gave an average degree of polymerization of n = 14. For fluorescence microscopy experiments, 0.2 mol % of either Texas Red 1,2-dihexadecanoyl-*sn*-glycero-3-phosphoethanolamine (TR-DHPE) or *N*-(6-tetramethylrhodaminethiocarbamoyl)-1,2-dihexadecanoyl-*sn*-glycero-3-phosphoethanolamine (TRITC-DHPE, both from Invitrogen, Karlsruhe, Germany) were incorporated into SOPC monolayers incorporating 5 mol % DS-PMOx14-Si. Glycerol was purchased from Carl Roth (Karlsruhe, Germany).

Vertical (Langmuir−Blodgett) Transfer of Monolayers. A cleaned substrate was immersed into the subphase before an appropriate amount of amphiphilic molecules in chloroform solution at 1 mg/mL was spread on the surface of a Langmuir trough (model 311D, Nima, Coventry, England) at 20 °C. After the solvent was evaporated, the film was compressed at 10 mm min^{-1} up to a surface pressure of 30 mN m^{-1}. The monolayer was transferred from the subphase by the vertical lifting of substrates (Langmuir−Blodgett method) at a transfer speed, v, while keeping the surface pressure constant. The transfer ratio was unity within the experimental error of 2%

Characterization of Transferred Monolayers. The stripe patterns in lipid/lipopolymer monolayers were characterized using fluorescence microscopy after the transfer with an inverted microscope (Carl Zeiss, Axiovert 200, Göttingen, Germany) equipped with a cooled CCD camera (ORCA ER, Hamamatsu Photonics, Herrsching, Germany). To determine the average stripe-to-stripe distance from each image, an intensity line profile perpendicular to the stripes was extracted over 140 μm. The positions of the manually selected maxima were fitted, and the slope of the linear fit yields the average distance (see Supporting Information). The standard deviations of the measured maxima from the ideal equidistant patterns are shown as error bars in Figures 4−6. The demixing of lipid-rich and lipopolymer-rich phases was semiquantitatively evaluated by the contrast ratio of the fluorescence intensity with respect to the background intensity from the nonilluminated area. The contrast ratio is defined as $(I_{max} - I_0)/(I_{min} - I_0)$:1 where I_0 is the background intensity value and I_{max} is the intensity recorded at the center of a stripe, whereas I_{min} is the intensity minimum between two stripes.

In Situ Imaging Ellipsometry. The local height profile near the three phase contact line was characterized with a Multiskop imaging ellipsometer (Optrel, Kleinmachnow, Germany), operating in the PCSA (polarizer−compensator−sample−analyzer) configuration. Using a microscope objective (M-Plan APO 10×, Mitutoyo, Neuss, Germany) and a position sensitive detector (EHD kamPro02, EHD imaging, Damme, Germany), the local height profile of the monolayer is obtained within the pixel resolution. The sample is illuminated by a HeNe laser (λ = 6328 Å) at an incidence angle of Θ = 50° (Figure 2), and a dipper holding the substrate was connected to a goniometer ring. A modified mirror holder (KMS/M, Thorlabs, Dachau, Germany) attached to the dipper allowed precise adjustment of the substrate angle. Due to geometric constraints of the setup, the dipping angle Ω was set to 75°. The height of the film balance was adjusted to see the onset of the meniscus in the ellipsometric image. The "nulling" conditions

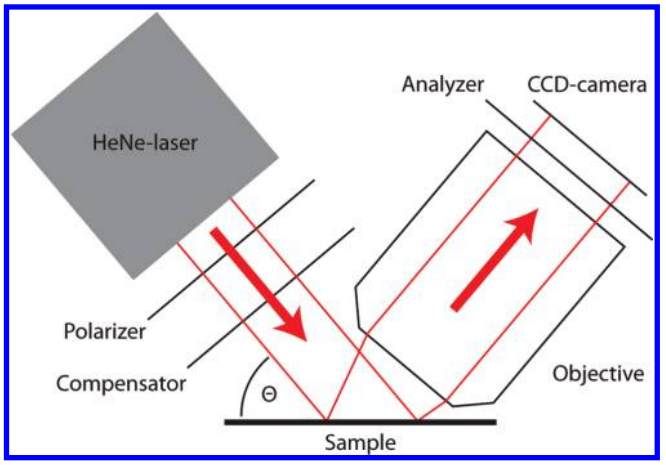

Figure 2. Schematic illustration of an ellipsometer combined with a Langmuir film balance. Monochromatic light (HeNe laser) passing through a polarizer and a compensator is reflected on the sample at an incidence angle, Θ. Reflected light is collected by a CCD camera through a microscope objective.

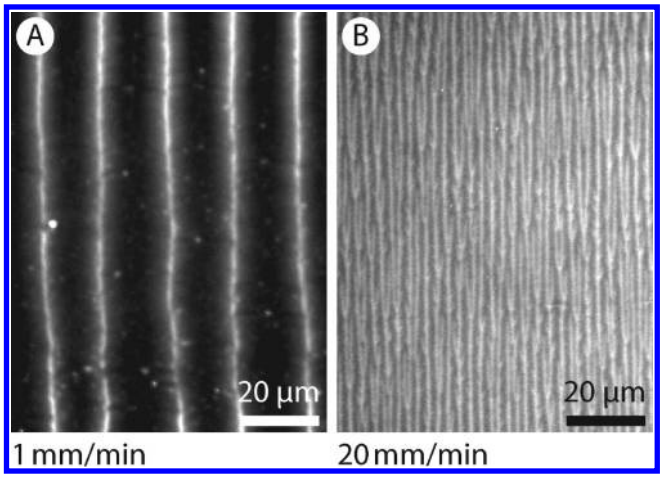

Figure 3. Fluorescence images from the monolayers transferred at (A) $v = 1$ and (B) $v = 20$ mm min^{-1}.

for zero intensity were fulfilled on the substrate surface so that the local height profile could be reconstructed from the pixel intensity in each order. It should be noted that this approach is valid only for small contact angles, where the increase in film thickness has to be less than half of the ellipsometric period over the pixel resolution.

In Situ Fluorescence Microscopy. To visualize the lateral demixing of lipid and lipopolymer molecules near the three-phase contact line during the film transfer, a self-built fluorescence microscope was coupled to the film balance. To create parallel light in the back focal plane of the microscope objective (M-Plan APO 10×, Mitutoyo, Neuss, Germany), the position of the objective was precisely adjusted prior to the experiment. Due to the diffraction limit, the spatial resolution of the setup ($\Delta x \sim 1.4\ \mu$m) can be calculated from the effective numerical aperture (NA = 0.28). A mercury lamp (EXFO X-cite 120, Mississauga, Ontario, Canada) illuminated the sample through an excitation filter (531/40 nm), and the fluorescence signal through an emission filter (593/40 nm) was collected on a CCD camera (Orca 285, Hamamatsu Photonics, Herrsching, Germany). All

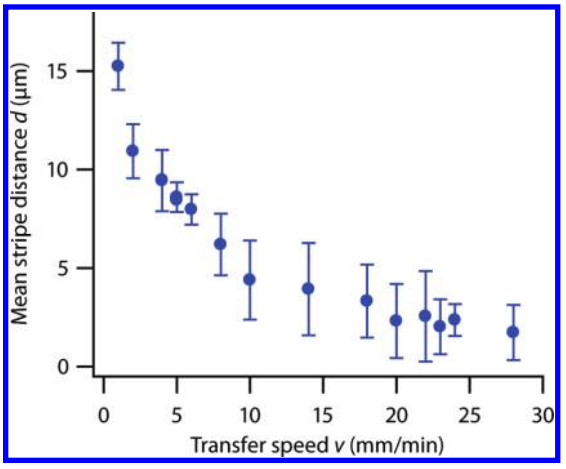

Figure 4. Stripe periodicity, d, as a function of transfer speed, v. Above $v = 30$ mm min^{-1}, stripe patterns are not discernible by fluorescence microscopy. Error bars show the standard deviation of the experimental values from the ideal regular pattern calculated from the line shape analysis.

the optical components were assembled in a cage system (Linos Photonics, Göttingen, Germany) and coupled to the detector arm.

RESULTS

To quantify the impact on the separation process, three well-controllable parameters were varied over the experimentally accessible range. The three parameters are transfer speed, v; subphase viscosity, μ; and the dipping angle, Ω (Figure 1).

Influence of Transfer Speed *v*. To investigate the influence of the transfer speed on the stripe patterns, the transfer speed, v, was varied from 1 mm min^{-1} to beyond 30 mm min^{-1}. Here, the other two parameters were set constant, that is, $\mu = 1$ mPa s and $\Omega = 90°$. Figures 3a and b represent the fluorescence micrographs of the same lipid/lipopolymer mixture transferred at $v = 1$ and $v = 20$ mm min^{-1}, respectively. As shown in the figure, an increase in v results in a clear decrease in the distance between neighboring stripes. Although the splitting and merging of stripe patterns could be observed along the direction of transfer, the stripes seem to maintain a finite equilibrium distance. It should be noted that the frequency of splitting/merging events seems to increase with the increase in speed, v. In fact, as presented in Figure 4, we observed a clear tendency of the equilibrium stripe−stripe distance to monotonically decrease with an increase in v. At $v > 30$ mm min^{-1}, no pattern could be discriminated within the microscopy resolution and contrast. On the other hand, we found that the stripe patterns are often perturbed by mechanical vibrations from the setup at $v < 5$ mm min^{-1}.

Influence of Subphase Viscosity. Red triangles in Figure 5 represent the contrast ratio plotted versus the subphase viscosity, μ, by mixing purified water ($\mu_{H_2O} = 1.00$ mPas) with glycerol ($\mu_{glycerol} = 7.80$ mPas).[20] As presented in the figure, a sharp decrease in the contrast ratio according to an increase in the subphase viscosity could be detected. At high viscositiy ($\mu > 2.5$ mPas), the stripe patterns could not be recognized any longer due to poor contrast. An alternative way to adjust the subphase viscosity is the variation of subphase temperature.[20] Although this allows a very limited range of subphase viscosities (blue triangles), it is possible to reach low viscosities with no risk of chemical perturbation, even below $\mu = 1$ mPas. It is noteworthy that the change in surface tension $\Delta\pi \leq 3.5$ mN m^{-1} by mixing

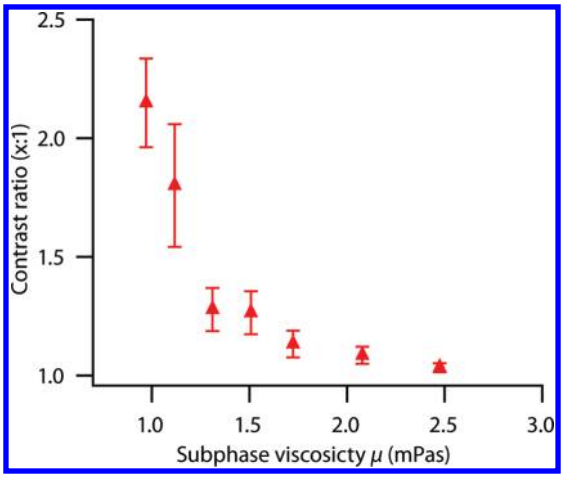

Figure 5. Contrast ratio as a function of subphase viscosity, μ. The definition of the contrast ratio is explained in the text.

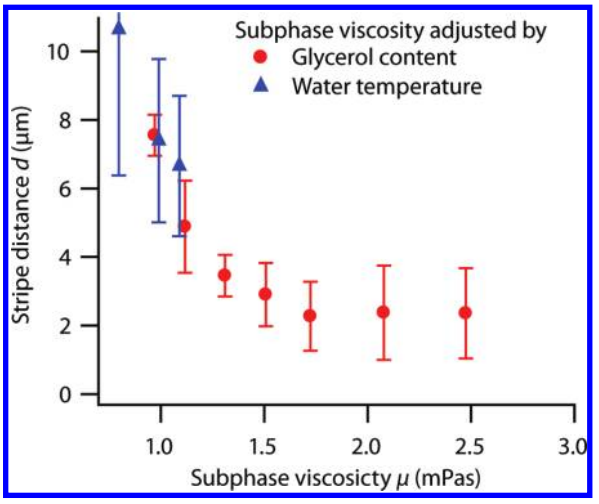

Figure 6. Stripe periodicity, d, as a function of subphase viscosity, μ. At $\mu > 2.5$ mPas, microscopic images showed a homogeneous distribution, making it impossible to determine a stripe-to-stripe distance. The subphase viscosity μ was varied either by mixing with glycerol (red circles) or changing the temperature (blue triangles). Error bars coincide with the standard deviation from an ideal periodic pattern.

glycerol plays no major roles because it is much smaller than the surface pressure during transfer (π = 30 mN m^{-1}).

Influence of Dipping Angle. The third parameter we varied is the dipping angle, Ω, which corresponds to a macroscopic contact angle between the substrate and the subphase. Here, the substrate was lifted up from the subphase at a constant speed (v = 5 mm min^{-1}) in the direction parallel to the substrate surface defined by Ω. Figure 7 represents the stripe periodicity d versus Ω = 15−150°. Within the experimental error (±1 μm) no remarkable influence of the dipping angle Ω on the stripe periodicity can be observed, suggesting that the measurement of local contact angles near the meniscus is necessary.

In Situ Imaging Ellipsometry Near Three Phase Contact Line. Figure 8A represents the ellipsometric image of a lipid/lipopolymer monolayer during the transfer. When the substrate is lifted at a constant speed, v = 5 mm min^{-1}, in the z direction (indicated by a vertical arrow), the film establishes a time-independent profile, as shown in Figure 8A (the corresponding movie is presented in the Supporting Information). In the case

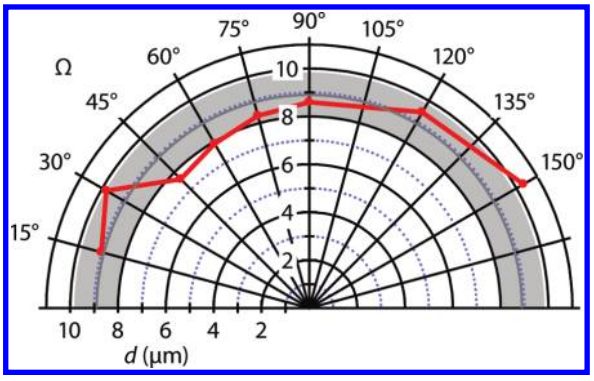

Figure 7. Stripe periodicity, d, plotted versus dipping angle, Ω (see Figure 1) between the substrate and the subphase. At a constant transfer speed (v = 5 mm min^{-1}) the stripe periodicity, d, shows no significant dependence on the dipping angle, Ω.

that the contact angle is small enough for the identification of intensity maxima/minima within the microscopy resolution, clear interference patterns can be detected when the film thickness decreases to micrometer order (horizontal arrow in Figure 8A). As presented in Figure 8B, the intensity integrated between two blue lines in panel A exhibits minima (indicated by green circles) corresponding to the ellipsometric periodicity of a water film in air (D = 290 nm). The height profile calculated from this result is reconstructed in Figure 8c.

The height profile is well approximated by a linear function, which allows the determination of a very small contact angle, α_r = 2.5°, near the three-phase contact line. From the ellipsometric images, we observed no heterogeneity in the contact angle corresponding to the thickness and periodicity of the stripe patterns, suggesting that the phase separation of lipids and lipopolymers is not caused by the local heterogeneity of the three-phase contact line. This is in contrast to previous reports on lipid−lipopolymer membranes, in which packing mismatch between polymer head groups and hydrocarbon chains[13,21] or random grafting of polymer chains to surfaces[22] caused topographic roughening of the membranes. It should be noted that the combination of a Langmuir film balance and an imaging ellipsometer is a powerful tool to spatially resolve the height profile of very thin (h < micrometers) liquid films near the interface, which would not be accessible with other experimental techniques.

In Situ Fluorescence Microscopy Near Three-Phase Contact Line. In addition to imaging ellipsometry, the dynamic pattern formation was monitored using in situ fluorescence microscopy. Figure 9A shows the fluorescence image near the meniscus captured during the transfer at a constant speed of v = 5 mm min^{-1}. The lipid−lipopolymer mixture showed no sign of phase separation when the subphase layer was thick. This seems consistent with the fact that lipids and lipopolymers are uniformly mixed at the air/water interface. When the film thickness decreased to a certain level, the lipid-rich and lipopolymer-rich phases were separated. This resulted in a stripe pattern with a regular periodicity (Figure 9B). It is technically not possible to obtain the critical film thickness at which the phase separation occurs, since fluorescence microscopy and imaging ellipsometry cannot be carried out at the same time. Nevertheless, the width of the transition region from a homogeneous lipid−lipopolymer mixture to a stripe pattern was found to be less than $\Delta z \sim 5$ μm. If we take the height profile of the same monolayer (Figure 8C), this Δz value coincides with a thickness change of $\Delta h \sim 230$ nm. This confirms that the observed mixing transition is not due to

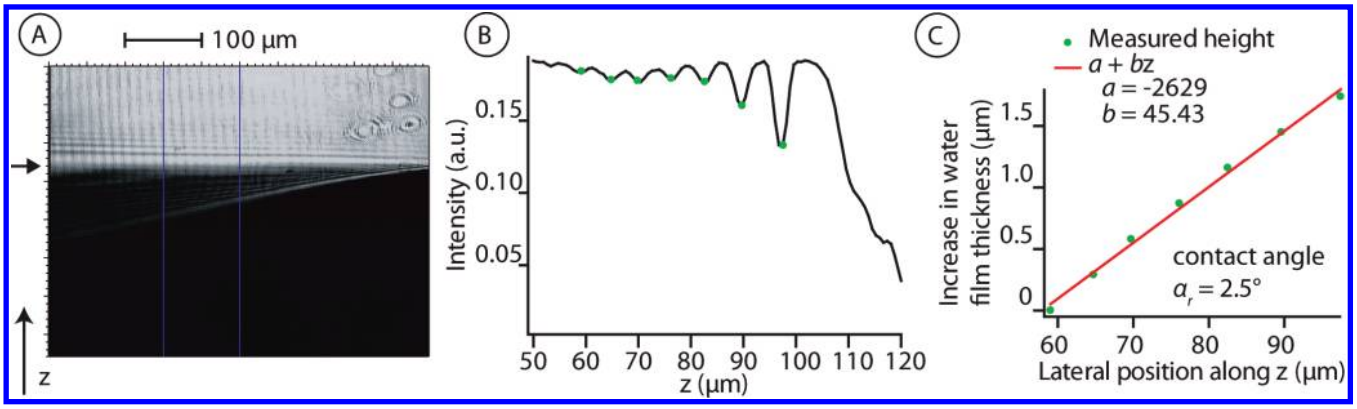

Figure 8. (A) Ellipsometric image near the three-phase contact line during the transfer at a constant speed v = 5 mm min^{-1}. The minima in the horizontal stripes perpendicular to the transfer direction coincide with the continuous increase in the film thickness, and the vertical stripes appearing in the upper part are optical artifacts. (B) Intensity profile along z integrated between the two blue lines in panel A exhibits seven clear minima (green circles), where the ellipsometric conditions are repetitively fulfilled. (C) The height profile of the film reconstructed from the interference minima in panel B plotted against the position along z. The height profile in this region can be approximated by a linear function that allows for the determination of a contact angle, α_r = 2.5°.

the escape of the sample from the focal plane. An apparent increase in fluorescence intensity beyond $\Delta h \sim 230$ nm can be attributed to the integrated fluorescence intensity over a meniscus with a large contact angle $\alpha_r \approx 30°$ (position marked with an arrow in Figures 8A and 9)

DISCUSSION

One of the commonly recognized examples of the formation of parallel stripe patterns near the interface would be so-called "tears of wine", which can be found near the bottom of a wine glass upon drying. This is caused by the chemical potential gradient along the fluid/fluid interface (Marangoni effect). Cazabat et al. designed the model systems based on heptane/dodecane mixtures and analyzed the length of the climbing film semiquantitatively.[23] However, such a "solutal" Marangoni effect can be excluded from the possible scenario, since there is no chemical potential gradient (temperature, surface pressure, film velocity) in our experimental system. A clear dependency of the stripe distance on transfer speed, v, and subphase viscosity, μ (Figure 1), suggests that hydrodynamic flows near the meniscus would play a key role in the pattern formation. Qualitatively, it is plausible that the slower draining of water underneath the monolayer would give lipid/lipopolymer mixtures longer time to undergo the phase separation. If one considers the influence of subphase viscosity, our finding can also be understood in terms of the mobility of molecules: the molecules can travel longer distance on a less viscous subphase.

Despite a clear indication of the influence of hydrodynamic flows near the meniscus, it is noteworthy that the macroscopic geometry of the sample has no effect. The dipping angle (Figure 1) coincides with the macroscopic contact angle at the three phase contact line, which can be described by the classical Young's equation. In fact, we observed significantly different macroscopic contact angles in the presence and absence of surfactant monolayers. For example, the thickness of a film, $h(z)$, at the dipping angle of Ω = 90° can be written using the following analytical expression:

$$h(z) = -\frac{a}{\sqrt{2}}\cosh^{-1}\frac{\sqrt{2}a}{z} + a\sqrt{\left(2-\frac{z^2}{a^2}\right)} + x_0$$

where a is the capillary constant and x_0 is the parameter determined by the contact angle.[24] As presented in Figure 8, the contact angle of a pure water film on a silicon substrate was found to be small, α_r = 2.5°, which can be accessible only with imaging ellipsometry at such a high precision. However, in the presence of lipid/lipopolymer monolayers, we obtained much larger contact angles (~30°, see the Supporting Information), corresponding to a decrease in the surface tension by the presence of surface active molecules[25] down to to $\Delta\gamma$ = (30.0 − 72.7) mN m^{-1} = −42.7 mN m^{-1}. Although the presence of lipid/lipopolymer molecules significantly increase the contact angle and guarantee the successful transfer of a monolayer with no loss of molecules,[26] its impact on the stripe periodicity is rather minor (Figure 7).

Within the framework of the lubrication theorem by deGennes,[27] one can estimate a maximum transfer velocity for the successful Langmuir−Blodgett transfer as a function of the contact angle, α_r:

$$V_{max} = \frac{\gamma}{36\sqrt{3}\cdot 12\mu\eta}\alpha_r{}^3$$

Namely, if one considers our sample geometry (identical to a so-called Landau and Levich geometry[28]), the transfer beyond this velocity results in the transfer ratio below unity. The maximum velocity for α_r = 30° ($V_{max} \approx$ 2000 mm min^{-1}) is far beyond all the experimental conditions, whereas the corresponding value for α_r = 2.5° (V_{max} = 1.1 mm min^{-1}) is lower than most of the experimental conditions.

To understand the physical mechanism, we started from the dimension analysis of our experimental systems. As we experimentally demonstrated, the stripe periodicity, d [L], is determined by the transfer velocity, v [L T^{-1}], and the subphase viscosity, μ [M L^{-1} T^{-1}]. Here, the combination of v and μ can be used to define shear stress, $\tau = v(\partial\mu/\partial y)$. It should be noted that only viscosity involves mass [M]; other physical parameters should be introduced to the model, such as surface viscosity of the monolayer [M T^{-1}], tension of the interface [M T^{-2}], etc. Due to a large number of possible combinations of parameters, it is difficult to create a physical model to quantitatively model our experimental findings.

Therefore, to analytically understand the mechanism of the observed pattern formation, we chose the Cahn−Hillard

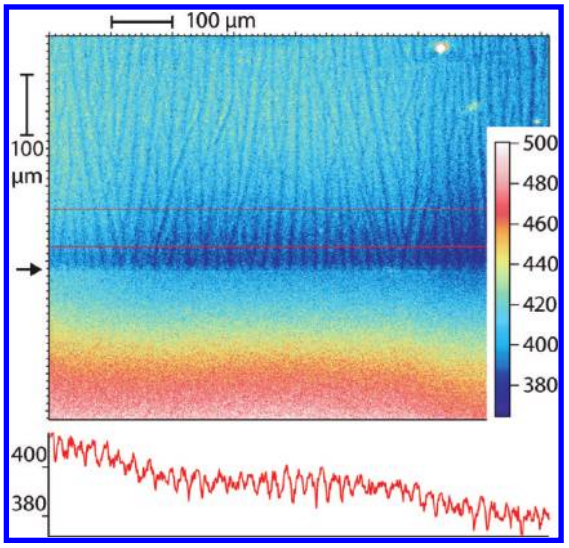

Figure 9. (A) In situ fluorescence micrograph near the three-phase contact line during the transfer of a lipid−lipopolymer monolayer at v = 5 mm min^{-1}. No separation of the two components can be observed below the arrow, whereas a clear stripe pattern is visible above this region. The width of the transition is less than $\Delta z \sim 5\ \mu$m, corresponding to a change in the film thickness of $\Delta d \sim 230$ nm. (B) The fluorescence intensity integrated between the two red lines in panel A. Periodic maxima correspond to the lipid-rich phase, and the minima, to the lipopolymer-rich phase.

equation,[29,30] which is a mathematical description of the phase separation in binary mixtures. Within this framework, Lifshitz and Slyozov reported that the time evolution of the domain size during the spinodal decomposition follows the power law $d \propto t^{1/3}$.[31] To test the validity of the model, we replotted the stripe periodicity, d, as a function of the time for the three-phase contact line to travel over 1 μm distance in a double logarithmic plot (Figure 10). The black line coincides with a fit with $d \propto t^{1/3}$, and the green line shows the χ^2 from this power law. As presented in the figure, the experimental results show very good agreement ($\chi^2 \leq 0.1$) at $t > 10$ ms, which corresponds to a transfer velocity of $v < 6$ mm min^{-1}. Beyond this transfer velocity, the experimentally measured stripe periodicities show a clear deviation from this power law ($\chi^2 > 0.3$). In fact, the results can be well fitted with a different exponent, $d \propto t^{4/5}$ (red line), suggesting another dominating mechanism for the separation of the constituents. Indeed, at transfer velocities beyond this threshold (e.g., $v = 20$ mm min^{-1}, Figure 3B), merging of stripes and emerging of new stripes can be frequently found. An explanation for the merging events requires at least a second independent variable that describes the evolution in transfer direction and, thus, time.

Transitions in growth rates of phase separating systems have been observed in different experiments and simulations[32] Experiments deal often with structures in three dimensions where binary or ternary mixtures in bulk are observed.[33−35] A number of reports also investigated the structure formation in two dimensions, which is normally driven by the dewetting of a thin film.[36,37] In contrast, our experiments take place in a quasi one-dimensional geometry. Unfortunately, it is experimentally impossible to decouple the shear exerted by the subphase from the time, to discover its role in the transition to the growth rate following another exponent, $d \propto t^{4/5}$. This may be a lead to an extension of the Cahn−Hilliard equation to gain deeper insights into the phase separation caused by fast dissipation.

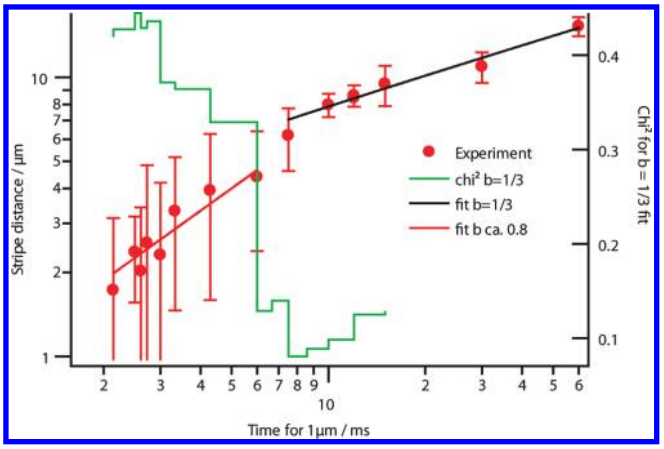

Figure 10. Experimental stripe distance plotted against time required to cover 1 μm at the transfer speed v (red dots). From the χ^2 of a power law fit with exponent $\beta = 1/3$ (green line), two regimes can be identified. For long times, the data fits well to a power law with exponent $\beta = 1/3$ (black line), whereas for short times, an exponent of $\beta \approx 0.8$ is more suitable (red line). Because of the large error in stripe distance determination, the slope in this regime may well be 1.

When the subphase is covered with amphiphiles, their presence does not seem to be dominant in the uppermost part of the meniscus. This changes at a water film thickness of $\approx$2 μm, where a kink in the meniscus leads to the much larger contact angle observed so far for successful Langmuir−Blodgett transfers.[26] From our observations using fluorescence microscopy, we conclude that this kink is the origin of the stripe pattern formation. The drag from the moving substrate drives the molecules at the air−water interface through this kink. The passage through the kink plays the role of a quench into the ordered phase for the lipid−lipopolymer mixture.

An obvious change occurs in the geometry while all other physical parameters (temperature, surface pressure, film velocity) are expected to be constant or change only slightly and steadily. From the orientation of the amphiphiles and the direction of the kink, a strong reduction of space in the alkyl chain region is apparent or, equivalent, an increase in area in the headgroup region. The average distance of the polymers is about four times their lateral extent, which allows us to exclude steric interactions of the polymers to dominate. If only curvature is responsible for a quench into the ordered phase, a phase separation between lipids and lipopolymers should occur in vesicles below a threshold size at the same conditions of temperature, surface pressure, and composition.

Following an argumentation by deGennes,[27] one can relate a contact angle to a maximum transfer velocity below which a Langmuir−Blodgett transfer is successful, that is, a transfer ratio on the order of 1, and above which the substrate is dip-coated, leaving a subphase film on the substrate, according to Landau and Levich.[28] When we calculate the maximum velocities for contact angles of 2.5° and 30°, we find us well below the dip-coating threshold for 30° at $v_{max} \approx 2000$ mm min^{-1}, whereas all presented experiments except one lie above $v_{max} \approx 1.1$ mm min^{-1} for 2.5°.

Plotting the experimental data of the stripe pattern formation against the time required to cover a distance of 1 μm in a double logarithmic plot, two regimes can be identified (see Figure 10). For short times (fast transfer speeds), a stronger increase in stripe distance is found than for slower transfer speeds (long times). For long timescales, the experimental findings can be explained by a power law with an exponent of $\beta = 1/3$. This suggests that

the stripe formation is due to a spinodal decomposition following the Cahn−Hilliard equation.[29,30] For the Cahn−Hilliard equation, Lifshitz and Slyozov showed that the growth of the observed structure follows $t^{1/3}$. For short times (fast transfer speeds), a different exponent was found ($t^{0.8}$), requiring another dominating mechanism for the separation of the constituents. Along with this change in growth rate, an increase in merging events during the transfer is observed.

In Figure 3B, the emergence of new stripes that join with other stripes shortly after in the course of transfer to retain the equilibrium distance can be seen. An explanation for the merging events requires at least a second independent variable that describes the evolution in transfer direction, coinciding with the temporal axis. Transitions in growth rates of phase-separating systems have been observed in different experiments and simulations[32] Experiments deal often with structures in three dimensions where binary or ternary mixtures in bulk are observed.[33−35] A number of reports also investigated the structure formation in two dimensions that is normally driven by the dewetting of a thin film.[36,37] In contrast, our experiments take place in a quasi one-dimensional geometry.

So far, we have not considered the effect of the shear exerted by the subphase on the monolayer upon transfer. We may expect that the shear force scales linearly with the velocity, $F_s \sim v \sim 1/t$. On the basis of the observation of a stationery interface during fast substrate removal—in other words, in the absence of a time-dependent instability—the shear force F_s should balance with the pinning force, F_p, of the lipid solution onto the substrate, $F_s = F_p$. Because the stripe width, d, is inversely proportional to the line density of the pinned points, we can deduce the relationship $d \sim t^1$. The shear is intrinsically coupled to the time in our experiments, making a separate observation impossible. The increase in shear with decreasing time enhances its relevancy for the growth regime with $\beta \approx 0.8$. Actually, the slope in this regime may well be 1 as a result of the large error in stripe distance determination. This may be a lead to an extension of the Cahn−Hilliard equation describing both the short time regime and the accompanying variation in merging frequency.

CONCLUSION

We reported the quantitative dependency of three preparative parameters on the characteristic periodicity of stripe patterns caused by the Langmuir−Blodgett transfer of lipid−lipopolymer monolayers. The film thickness near the three-phase contact line during transfer was measured by an imaging ellipsometer coupled to a film balance. The in situ ellipsometric imaging allows for the determination of an extremely small contact angle of 2.5° close to the substrate and excludes the contribution of a local fluctuation of the meniscus. The lateral phase separation of lipids and lipopolymers near the meniscus during the film transfer was monitored by fluorescence microscopy, confirming that the width of the transition from the homogeneous mixture to stripes is below 5 μm. The mechanism of the phase separation was interpreted as the spinodal decomposition within the framework of the Cahn−Hillard equation. The stripe periodicity observed at slow transfer velocity ($v < 6$ mm min^{-1}) showed good agreement with the theoretically predicted power law $d \propto t^{1/3}$.

ASSOCIATED CONTENT

Supporting Information. Ellipsometric movie taken during LB transfer with 5 mm min^{-1}. Movie of a side view of immersed substrate during compression of LB film. Determination of stripe distance. This material is available free of charge via the Internet at http://pubs.acs.org.

AUTHOR INFORMATION

Corresponding Author

*Phone: +49 6221 54 4917. Fax: +49 6221 54 4918. E-mail: Tanaka@uni-heidelberg.de.

ACKNOWLEDGMENT

We thank the German Science Foundation (Ta259/5, German-Japanese Collaborative Project) for financial support. M.T. is a member of the German Excellence Cluster "Cell Network", Helmholtz Program "BioInterface", and BIOQUANT. P.C.S. thanks the JSPS for a fellowship and Dr. H. Wada and Prof. T. Ohta for fruitful discussions.

REFERENCES

(1) Singer, S. J.; Nicolson, G. L. *Science* **1972**, *175*, 720.
(2) Vereb, G.; Szöllosi, J.; Matkó, J.; Nagy, P.; Farkas, T.; Vígh, L.; Mátyus, L.; Waldmann, T. A.; Damjanovich, S. *Proc. Natl. Acad. Sci. U.S.A.* **2003**, *100*, 8053.
(3) Jacobson, K.; Sheets, E. D.; Simson, R. *Science* **1995**, *268*, 1441.
(4) Jacobson, K.; Mouritsen, O. G.; Anderson, R. G. W. *Nat. Cell Biol.* **2007**, *9*, 7.
(5) Reiter, G. *Phys. Rev. Lett.* **1992**, *68*, 75.
(6) Reiter, G.; Sommer, J.-U. *Phys. Rev. Lett.* **1998**, *80*, 3771.
(7) Sackmann, E. *Science* **1996**, *271*, 43.
(8) Tanaka, M.; Sackmann, E. *Nature* **2005**, *437*, 656.
(9) Purrucker, O.; Förtig, A.; Jordan, R.; Tanaka, M. *ChemPhysChem* **2004**, *5*, 327.
(10) Wagner, M. L.; Tamm, L. K. *Biophys. J.* **2000**, *79*, 1400.
(11) McGillivray, D. J.; Valincius, G.; Vanderah, D. J.; Febo-Ayala, W.; Woodward, J. T.; Heinrich, F.; Kasianowicz, J. J.; Lösche, M. *Biointerphases* **2007**, *2*, 21.
(12) Diaz, A. J.; Albertorio, F.; Daniel, S.; Cremer, P. S. *Langmuir* **2008**, *24*, 6820.
(13) Deverall, M. A.; Gindl, E.; Sinner, E.-K.; Besir, H.; Ruehe, J.; Saxton, M. J.; Naumann, C. A. *Biophys. J.* **2005**, *88*, 1875.
(14) Seitz, P. C.; Reif, M. D.; Konovalov, O. V.; Jordan, R.; Tanaka, M. *ChemPhysChem* **2009**, *10*, 2876.
(15) Purrucker, O.; Förtig, A.; Jordan, R.; Sackmann, E.; Tanaka, M. *Phys. Rev. Lett.* **2007**, *98*, 078102.
(16) Purrucker, O.; Förtig, A.; Lüdtke, K.; Jordan, R.; Tanaka, M. *J. Am. Chem. Soc.* **2005**, *127*, 1258.
(17) Kern, W.; Puotinen, D. A. *RCA Rev.* **1970**, 187.
(18) Persigehl, P.; Jordan, R.; Nuyken, O. *Macromolecules* **2000**, *33*, 6977.
(19) Jordan, R.; Martin, K.; Räder, H. J.; Unger, K. K. *Macromolecules* **2001**, *34*, 8858.
(20) Segur, J. B.; Oberstar, H. E. *Ind. Eng. Chem.* **1951**, *43*, 2117.
(21) Ahrens, H.; Bækmark, T. R.; Merkel, R.; Schmitt, J.; Graf, K.; Raiteri, R.; Helm, C. A. *ChemPhysChem* **2000**, *1*, 101.
(22) Naumann, C. A.; Prucker, O.; Lehmann, T.; Rühe, J.; Knoll, W.; Frank, C. W. *Biomacromolecules* **2002**, *3*, 27.
(23) Vuilleumier, R.; Ego, V.; Neltner, L.; Cazabat, A. M. *Langmuir* **1995**, *11*, 4117.
(24) Landau, L. D.; Lifshitz, E. M. *Fluid Mechanics*, 2nd ed.; Butterworth Heinemann: Woburn, MA, 1987; Vol. 6.
(25) Yaminsky, V.; Nylander, T.; Ninham, B. *Langmuir* **1997**, *13*, 1746.
(26) Cerro, R. L. *J. Colloid Interface Sci.* **2003**, *257*, 276.
(27) de Gennes, P. G. *Colloid Polym. Sci.* **1986**, *264*, 463.

(28) Landau, L.; Levich, B. *Acta Physicochim. U.R.S.S.* **1942**, *17*, 42.
(29) Cahn, J. W.; Hilliard, J. E. *J. Chem. Phys.* **1958**, *28*, 258.
(30) Bestehorn, M. *Hydrodynamik und Strukturbildung*; Springer: Berlin, 2006.
(31) Lifshitz, I. M.; Slyozov, V. V. *J. Phys. Chem. Solids* **1961**, *19*, 35.
(32) Bray, A. J. *Adv. Phys.* **2002**, *51*, 481.
(33) Takeno, H.; Hashimoto, T. *J. Chem. Phys.* **1997**, *107*, 1634.
(34) Butler, M. F.; Heppenstall-Butler, M. *Biomacromolecules* **2001**, *2*, 812.
(35) Cabral, J. T.; Higgins, J. S.; Yerina, N. A.; Magonov, S. N. *Macromolecules* **2002**, *35*, 1941.
(36) Green, P. F. *J. Polym. Sci., Part B: Polym. Phys.* **2003**, *41*, 2219.
(37) Chung, H.-j.; Composto, R. J. *Phys. Rev. Lett.* **2004**, *92*, 185704.